Chapter 8
Ultrastructure Imaging: Imaging and Probing the Structure and Molecular Make-Up of Cells and Tissues

Matthias Amrein

"New directions in science are launched by new tools much more often than by new concepts"

- Freeman J. Dyson (Princeton)

Abstract The past few years have seen dramatic improvements in life science microscopy. This chapter points out important recent developments that will probably affect many researchers in this field. Super-resolution fluorescence light microscopy allows for ultrastructure imaging of living cells. In electron tomograms, macromolecular complexes can be directly identified by shape without the need for labeling. Atomic force microscopes image isolated elements of the ultrastructure, including membranes and macromolecules, at submolecular resolution. This technology also makes molecular interactions directly accessible by measuring binding forces. In the chapter, new concepts are discussed in relation to current mainstream techniques. We will end with a brief discussion of novel concepts that could allow the molecular compositions of cells and tissues to be mapped in an unbiased, systematic way.

Introduction

Cells are organized into compartments and functional units down to the macromolecular level. The frameworks of these functional and structural units are either complexes containing only proteins, protein complexes that also include nucleic acids, or protein complexes that also include lipids. The recently completed map of the human genome as well as the systematic mapping of the proteins expressed

M. Amrein
Microscopy and Imaging Facility, Department of Cell Biology and Anatomy, Faculty of Medicine, University of Calgary, 3330 Hospital Drive N.W., Calgary, Alberta, T2N 4N1 Canada, e-mail: mamrein@ucalgary.ca

C.W. Sensen and B. Hallgrímsson (eds.), *Advanced Imaging in Biology and Medicine*.

in tissues and cells that this initiated (proteomics) are part of a concerted effort to rapidly advance our understanding of the functions of macromolecular functional units and the cell. However, proteomics only reveals the basic inventory of a cell, and this inventory is insufficient to explain the function of each element and the orchestration of the components. Attempting to understand life without observing the structures behind the functions is inconceivable. At the cellular and subcellular level, microscopy plays this important role by putting the molecular elements into their structural context. The pace of discovery of these elements has increased substantially via proteomics and this has also substantially increased the need for more and more sophisticated microscopy in the recent years.

Microscopy has existed for more than 500 years, and started with the simple magnifing glass. Work with the magnifying glass reached its peak in the 1600 s with the work of Anton von Leeuwenhoek, who was able to see single-celled animals and even bacteria. However, simple magnifiers had severe limitations in terms of illumination, image distortions, and resolution. The following sections describe how these limitations were gradually overcome by the introduction of increasingly ingenious "compound" light microscopes, thus achieving our first insights into the ultrastructure of a cell, or by exchanging the light—part of the electromagnetic spectrum—for a beam of electrons, thus reaching submolecular resolution.

Until very recently, the resolving power of the light microscope appeared to be invariably limited by diffraction. However, this barrier has now been surmounted to a degree, allowing elements of the ultrastructure of a cell to be well resolved. For now, the one dominant remaining limitation of light microscopy remains the need for labeling. Electron microscopy too has seen a dramatic change due to the implementation of tomographic data acquisition over the past few years. The resolving power of these microscopes is limited to the level where large molecular complexes are recognizable by shape. Higher resolutions appear to be invariably excluded because of the damage caused to the sample by the illuminating beam.

Not all microscopes depend on the emission of radiation and the subsequent recording of it at a distance from the sample using lenses. The atomic force microscope (AFM) is part of a family of microscopes that rely on an effect that is only present when a physical probe is in the immediate proximity of the sample, and this will be discussed below as well. It sometimes offers better resolution (or a better "signal-to-noise" ratio) than an electron microscope. More importantly, it can be used as a nanorobot to perform local experiments on cells or single molecules.

This chapter is not intended to be a history of microscopy, nor an exhaustive technical review. It points out important recent developments in life science microscopy that will probably affect many of those in this segment of the research community. The new concepts are described from the perspective of current mainstream techniques. We will end with a brief discussion of novel concepts that might allow the molecular compositions of cells and tissues to be mapped in an unbiased, systematic way.

Recent Developments in Light Microscopy

Recent developments have extended the resolution of light microscopy into the subcellular and ultrastructure range. Most of the improvements relate to fluorescent light microscopy and include a large and rapidly increasing set of fluorescent dyes and ingenious new means to improve the resolution and sensitivity at which the fluorescently labeled structures within a cell or tissue can be detected. Some of the most prominent of these developments will be discussed below. However, not everything can be fluorescently labeled, and improvements have also occurred in the visualization of unstained cellular structures by regular transmission light microscopy of unlabeled samples. One such development, hollow cone illumination by a "cardioid annular condenser" from CytoViva, is addressed below. First, we will briefly introduce some of the basic principles of light microscopy, an understanding of which is needed in order to comprehend the recent improvements in this field.

Basic principles of light microscopy (Fig. 8.1): The objective (together with a tube lens inside the microscope) produces a magnified image of the specimen inside the optical path leading up to the eyepiece or a camera. The image is then seen after being further magnified through the eyepiece or projected onto the light-sensitive chip of a camera. The objective is the most prominent optical component of the microscope. Its basic function is to collect the light passing through the specimen and then to project an accurate, magnified image of the specimen. Objectives have become increasingly sophisticated in terms of corrections for image distortions. A single magnifying lens focuses light of different wavelengths (colors) into different focal spots (chromatic aberration), and also focuses light entering the lens far from the optical axis into a different focal spot than light traveling through the central region of the lens (spherical aberration). Furthermore, not all of the specimen seen through the lens is in focus at the same time; when the center is in focus the periphery is not, and vice versa (field curvature). Corrections are indispensable when attempting to achieve the highest possible resolution.

The most basic correction is established by using "achromatic" objectives, which are corrected for chromatic aberration at two wavelengths (red and blue) and for spherical aberration at the color green but not for field curvature. Planapochromatic objectives yield the highest level of correction by eliminating chromatic aberration and spherical aberration almost entirely. They also produce "flat" images (without field curvature).

The resolving power of even the best-corrected objective is "diffraction limited" irrespective of whether fluorescence light or regular transmission light microscopy is being performed. As a consequence, the useful magnification is limited, and any additional magnification does not result in a more detailed image. When light from a specimen passes through the objective and is reconstituted as the image, the small features of the specimen appear in the image as small disks (Airy disks) rather than as points because of diffraction. Equally, sharp edges in the specimen appear blurred in the image. The function that describes the spreading of a point or edge in the specimen into a disk or blurred edge in the image is called the point spread function (PSF) and depends notably on the objective but also on other optical elements of the

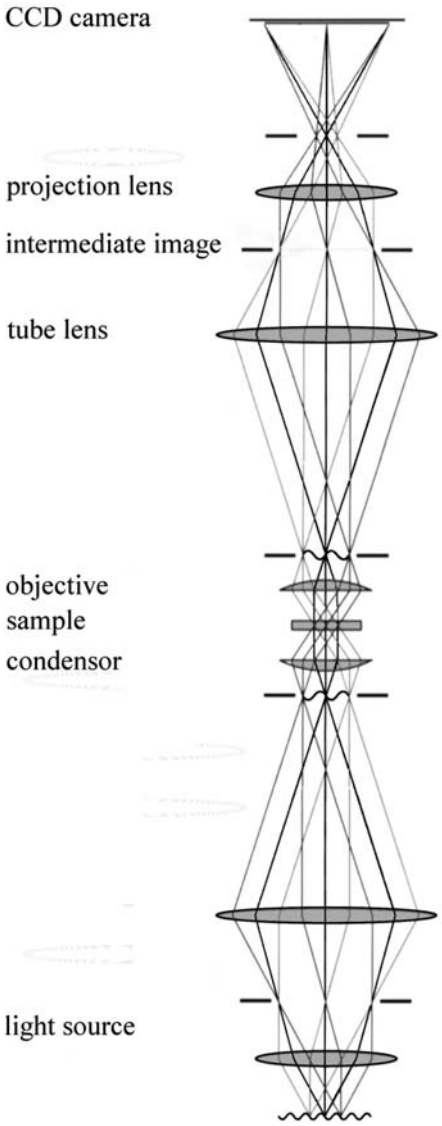

Fig. 8.1 Ray diagram of a regular transmitted light microscope in Koehler illumination (adapted from Hammond and Heath 2006). The hot filament of the light source is denoted by *a sinusoidal line*. It radiates light in all directions. Three representative rays from three different locations on the filament are shown. Whenever rays from a common origin on the filament (indicated by the same shade of *gray*) cross, the filament is in focus. Rays emanating from a common spot in the sample recombine at the plane of the intermediate image and (further enlarged) at the camera plane

microscope. Disks that are close to each other in the image, representing objects in close proximity in the specimen, will overlap and eventually become indiscernible. The better the microscope, the smaller the Airy disks and the finer the detail of the specimen discernible. Objectives that yield better correction result in smaller Airy disks than objectives that produce less correction, and so they have higher resolving power. Numerical aperture (NA) is another factor that determines the diameter of the Airy disk. The NA is a measure of the opening angle of the objective. It quantifies the ability of an objective to include rays of light from all directions from the specimen. Objectives with lower opening angles include a narrower cone of light compared to objectives with higher angular apertures. Specifically, the numerical aperture (NA) is given by $\mathrm{NA} = n\sin(\alpha)$, where n is the index of refraction of the material between the specimen and the front lens of the objective ($n = 1$ for air with a "dry" lens, $n = 1.5$ for the oil in an oil immersion lens, and $n = 1.3$ for a water immersion lens). $\sin(\alpha)$ is the sine of half the opening angle of the objective. An objective with a higher NA will produce narrower Airy disks than an otherwise similar counterpart with a lower NA. The resolution power of the best dry lens is by definition lower than that of a water or oil immersion lens because of its inherently lower NA. Another factor influencing the resolving power of a microscope is the wavelength of the light. The shorter the wavelength, the higher the achievable resolution. In summary, the traditional resolution criterion for a light microscope is the Rayleigh criterion r, where $r = 0.61\lambda/\mathrm{N.A.}$ r is the smallest distance between objects that still are discernible in the image; λ is the wavelength of the light (Fig. 8.2).

Cardioid annular condenser illumination: Despite the success of fluorescence light microscopy, transmission light microscopy (TLM) is also still important in the life sciences. For example, the evaluation of stained tissue sections is ubiquitous in animal and human pathology. When used in combination with fluorescence light microscopy, TLM allows some of the elements of the ultrastructure of the cell with which the fluorescently labeled elements associate to be identified. In this case, the highest possible resolution is of particular interest, as many elements of the ultrastructure of the cell are only just resolvable by regular TLM or cannot be visualized this way. In TLM, the light enters the sample from a source on the opposite side of the objective, and the quality and numerical aperture of the objective are not the only concerns in high-resolution imaging; the illumination light path needs to be factored in too. In the common approach known as "Koehler illumination," a lens projects an enlarged image of a light source (e.g., a hot filament) into focus at the front focal plane of a condenser. The condenser is a lens system with distortion corrections that should match the quality of the objectives. The light emerging from the condenser travels through the specimen in parallel rays from every angle within the numerical aperture of the condenser such that the sample is evenly illuminated from all directions. To fully realize the numerical aperture of the objective, the condenser must have a matched NA. This may require that the condenser also needs to be used with immersion oil. In this configuration, the diffraction-limited resolution (Rayleigh criterion) is $r \sim 240\,\mathrm{nm}$ at best. Note that this is insufficient for resolving most cellular ultrastructure.

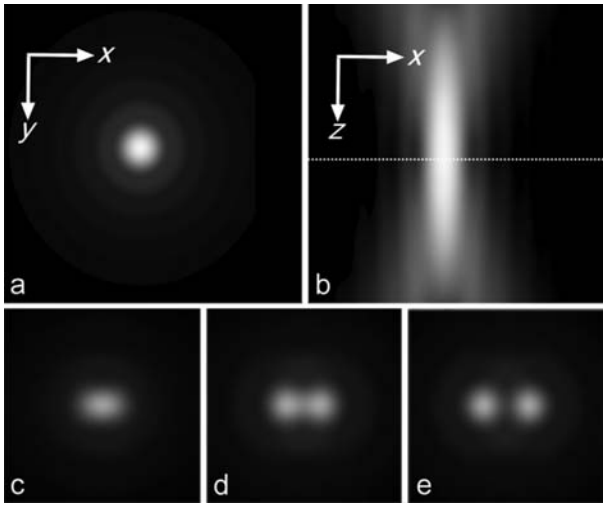

Fig. 8.2 (**a**) Even an infinitesimally small structure in a sample is spread out into an Airy disk in the image plane (x, y plane), according to the point spread function (PSF) of the optical system. (**b**) The spread is even more pronounced along the optical axis (z direction; the image plane is indicated by a *dashed line*). No feature of the sample is imaged beyond the precision permitted by the PSF and the resolution power is thus limited. The lower row shows the Airy disks of two structures too close to each other to be resolved (**c**); far enough apart to be barely resolved (**d**), and well resolved (**e**)

Higher resolution and better contrast can now be obtained by modifying the light path used in Koehler illumination. CytoViva markets an optical illumination system that replaces the standard condenser with a cardioid annular condenser (Fig. 8.3). In this configuration, the sample is illuminated by a hollow cone of parallel rays. This improves optical resolution; indeed, a resolution of 90 nm has been demonstrated. This increased resolution results from the narrower Airy disk that arises under coherent illumination for an annular aperture compared to that arising from the circular aperture under regular Koehler illumination (Vainrub et al. 2006).

Cardioid annular condenser illumination also appears to inherently provide contrast for unstained "transparent" cell or tissue samples (through a mechanism that is yet to be described). Note that regular Koehler illumination requires one to either stain the samples or employ methods to enhance the contrast of the unstained samples, such as differential interference contrast (DIC).

Optical sectioning microscopy; confocal and deconvolution light microscopy: Fluorescence light microscopy is arguably the most important microscopy used in the life sciences. In the following sections, we first describe technical advancements that have been instrumental to its success and then point out new directions that can take this microscopy into the realm of the ultrastructure of the cell (Conchello and Lichtman 2005).

In fluorescence light microscopy, the light used to excite fluorescent dyes is focused into the sample by the same objective that also collects the fluorescence

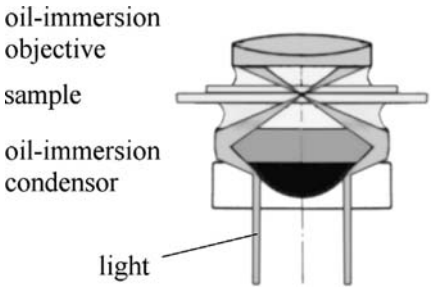

Fig. 8.3 Cardioid annular condenser. A hollow cylinder of light is deflected by a sperical mirror (*black*) outwards and is reflected back in again by another mirror onto the sample in a hollow cone. To ensure a large angle of illumination, the condensor is optically coupled to the glass slide of the sample with immersion oil. The light penetrating the sample and the coverslip enters the oil immersion objective far from the optical axis. This set-up improves resolution and offers a strong contrast for unstained samples that are barely visble in regular transmitted light micrsocopy

produced by the dyes. This configuration is termed epi-illumination. As with Koehler illumination, a cone of (excitation) light enters the sample. The fluorescent light is separated from the illuminating light by a filter set (Fig. 8.4).

Unfortunately, the illuminating light causes the excitation of not only the fluorescent dyes within the focal plane but also the fluorophores well above and below this plane. This is because the intensity of the illumination light does not drop sharply below and above the focal plane, according to the PSF of the optical system in the axial direction (see Fig. 8.2b). The haze caused by this out-of-focus light strongly obscures the in-focus image and reduces the contrast.

Optical sectioning microscopy, achieved using either specific hardware or through computational methods, eliminates the out-of-focus light and thus strongly improves the contrast in the images. It constitutes the single most important improvement in this type of microscopy. Moreover, for all methods, rather than taking a single image of the sample region, a stack of images ("optical sections" or frames) are acquired over the depth of the sample. Three-dimensional reconstructions of the sample volume are then obtained by combining the individual images from the stack in the computer.

In laser scanning confocal microscopy (LSCM, also termed LSM), optical sections of a sample are obtained by raster scanning an individual image frame at a given focal height, then moving incrementally to a new focal height and acquiring the next frame, etc., until a full stack of images has been acquired. The excitation light is brought into focus within the sample, and this focal spot is scanned. The fluorescent light produced travels back through the objective. It is separated from the excitation light by a filter and projected into a light detector. The image is then produced in the computer from the fluorescence intensity for each location within the image frame. To prevent out-of-focus light from entering the detector (i.e., fluorescence produced in the illumination cones above and below the focal spot), the fluorescence light stemming from the focal spot is brought into focus in front of the detector. At this location, the light must pass through a pinhole aperture

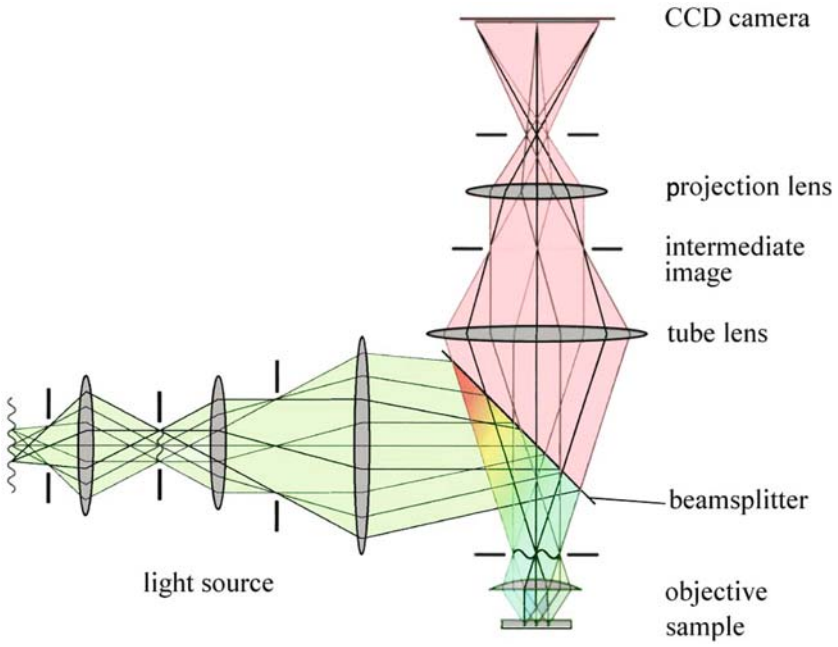

Fig. 8.4 Ray diagram of a fluorescence light microscope (adapted from Hammond and Heath 2006). Note that the illumination (excitation) light enters the sample from the same side as it is collected (epi-illumination). The excitation light (*denoted green*) and the emitted fluorescence (*denoted red*) are inherently of different wavelengths. This allows one to stop any excitation light from entering the camera by using a dichroic mirror (beam splitter) as well as additional filters (not shown)

that is just large enough to get through. Fluorescence produced above or below the illumination spot inside the sample will reach the pinhole somewhat out of focus and will thus spread out. Most of it will therefore be blocked out by the pinhole aperture. Because the illumination spot inside the sample and the fluorescence emanating from this spot at the pinhole in front of the detector are always in focus together, this type of microscopy is called "confocal." The pinhole not only eliminates the out-of-focus light and so strongly improves contrast; it also leads to a noticeable, albeit small, improvement in resolution.

The first commercial LSCM was designed at the MRC Laboratory of Molecular Biology in Cambridge, UK (Biorad MRC 600; BioRad Laboratories, Hercules, CA, USA) and scanned a single illumination spot using mirrors. One of the few drawbacks of this type of LSCM, particularly for live cell imaging, is slow image acquisition due to the time needed to scan an image frame with a single laser spot. In comparison, in a "wide-field" (i.e., regular) microscope, the entire image is acquired simultaneously, in which case the frame rate of the camera determines the speed. However, the problem of long acquisition times has now been overcome in another implementation of the confocal microscope, the "spinning-disk confocal microscope" (SDCM) (Fig. 8.5). Here, the image acquisition rate may be up to

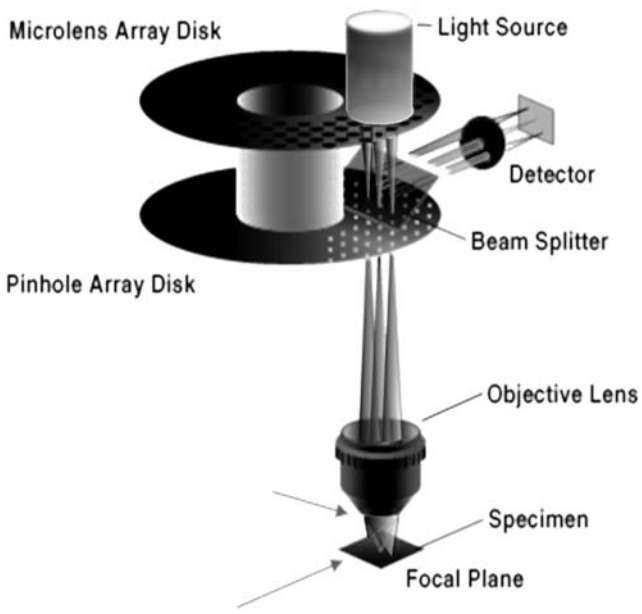

Fig. 8.5 Principle of the microlens-enhanced SDCM. An expanded, collimated laser beam illuminates the upper disk, which contains ∼20,000 microlenses. Each lens focuses an individual beam onto a corresponding pinhole. The beams passing through each of the pinholes fill the aperture of the objective lens and are focused on the focal plane. The fluorescence generated from the specimen for each beam is focused back onto its pinhole, deflected by a dichroic mirror and focused into the image plane in the camera. As compared to conventional LSCM, multibeam scanning requires a significantly lower level of light intensity per unit area, which results in significantly reduced photobleaching and phototoxicity in live cells (adapted from http://www.yokogawa.com)

2,000 frames per second (CSU-X1, Yokogawa Co., Tokyo, Japan). In SDCM, rather than having a single laser spot scanning the sample, up to a thousand spots within a single image frame at any given time move simultaneously through the sample. This is accomplished by using a rapidly spinning disk (the Nipkow disk) that contains up to about 20,000 pinholes which cut perpendicularly through the illumination beam and break it up into individual, fast-moving beams. Newer set-ups use two disks on a common axis that spin together. One disk contains as many microlenses as there are pinholes in the other disk. Each of these lenses focuses part of the illuminating light into the corresponding pinhole on the other disk, where it is focused by the objective into the sample. The fluorescence from each illumination spot travels back into the objective, is focused into its corresponding pinhole, and progresses into a CCD (charge-coupled device) camera or an eyepiece. The pinholes reject the out-of-focus light and only allow the in-focus light into the camera. Image formation is so fast that it appears to be instantaneous, as in wide-field microscopy. Another advantage of the spinning-disk system over single-spot LSCM, particularly for live cell imaging, is the lower light intensity required per unit area of the sample. This results in

reduced photobleaching and lower phototoxicity, both of which are problems that arise with a single spot scanner.

An alternative way of removing out-of-focus light from the LSCM is "digital deconvolution microscopy." A stack of regular wide-field fluorescence images are acquired, and the out-of-focus light is removed from each optical section afterwards by computational methods rather than by using pinholes. This method was derived based on information about the process of image formation. The earliest and computationally least demanding implementation is termed "nearest neighbors deconvolution." It subtracts the blur stemming from the sections immediately adjacent to (above and below) the current section. The method works well if a specimen consists of small fluorescent spots or thin filaments, but fails for larger fluorescent areas such as cell membranes or larger volumes. In these latter cases, it breaks the contiguous structures up into many spots. A more sophisticated method, termed "frequency-based deconvolution," first decomposes images computationally using a Fourier transform into series of periodic structures of different frequencies, amplitudes and phases (where smaller details give rise to higher frequencies and large structures to low frequencies). The frequency components of a microscopic image represent the "true frequency components of the specimen" multiplied by the "optical transfer function" (OTF) of the microscope. The OTF is the Fourier-transformed point spread function of the microscope. Hence, dividing the frequency components of the image by the OTF should undo the blur produced by the microscope within the resolution limit imposed by the impracticality of dissecting the overlapping Airy disks from objects too close to each other. When they are then superimposed (using a reverse Fourier transform), these corrected periodic structures should give rise to a corrected image. Unfortunately, this operation is not directly applicable because the OTF is zero for high frequencies (small details), beyond the resolution limit of the microscope. Division by zero is undefined. This makes more sophisticated methods necessary that circumvent division by zero, but unfortunately all of these introduce various image artefacts. These artefacts are minimized by also including information obtained a priori about the image in "constrained deconvolution" algorithms. These algorithms work iteratively and are typically time-consuming and computationally demanding. Different implementations are distributed commercially by Applied Precision, Scanalitics, AutoQuant Imaging, or are freely available (http://www.omrfcosm.omrf.org).

Super-resolution light microscopy: Currently, fluorescence microscopy is undergoing another revolution and a number of new methods have improved resolution by a degree that only recently was considered impossible. As a result, true ultrastructure imaging has now become possible. However, this super-resolution optical microscopy has so far provided only a few novel biological results. However, this situation is bound to change as the technologies become more readily available. Some of the new methods, with one prominent example being STED (stimulated emission depletion, see below), are technically demanding and require specialized equipment that is only now becoming commercially available. Another method of achieving super-resolution imaging only requires a regular microscope and depends on specialized but easily obtainable fluorescent labels, as well as special microscope

control and data processing (this method has been published by three independent groups as STORM, PALM and FPALM, respectively).

STED uses a set-up similar to the laser scanning confocal microscope described above, but employs a sequence of two laser pulses for each point in the scanned region (Schmidt et al. 2008: Vainrub et al. 2006; Willig et al. 2006) (Fig. 8.6). First there is a pulse to excite any fluorophores in the focal spot, just as in regular LSCM (excitation pulse). Immediately following this, a second pulse with a slightly longer wavelength returns the excited fluorophores to their previous nonfluorescent ground states (depletion pulse). Unlike the excitation pulse, the depletion pulse is not focused into a spot. Instead, it is shaped into a cylinder that tightly encloses and cuts into the excitation spot, thus narrowing the region from which the fluorescence emanates down to a few nanometers in diameter. Thus, the lateral resolution has been improved by close to an order of a magnitude! The 20–70 nm lateral resolution realized with STED has been used to map proteins inside cells and on the plasma membrane.

More recently, the inventors of STED have come up with a STED scheme where an excitation spot is surrounded not just in the sample plane (x, y), but also in the axial direction (z), so that an isotropic fluorescent spot about 50 nm in diameter is achieved (Schmidt et al. 2008) (Fig. 8.6). For this, the sample was mounted in-between two oil immersion objectives positioned opposite to each other in a set-up termed 4-pi (due to the theoretical numerical aperture of 4-pi, or 360°, offered by such system). STED is now being offered by Leica Microsystems (TCS STED). It is integrated into the confocal platform TCS SP5. Note that the current commercial system is not a 4-pi microscope, so the improvement achieved by STED in this case will occur in the image plane only. However, Leica also offers a 4-pi system, so one can reasonably expect the full three-dimensional system to become commercially available too.

STORM (stochastic optical reconstruction microscopy) (Rust et al. 2006; Perfect Storm 2008; Vainrub et al. 2006; Huang et al. 2008), photo-activated localization microscopy (PALM) (Betzig et al. 2006; Manley et al. 2008; Shroff et al. 2008), and fluorescence photo-activated localization microscopy (FPALM) (Hess et al. 2006, 2007) are acronyms for essentially the same simple and yet ingenious method for accomplishing super-resolution in light microscopy (Fig. 8.7). The three implementations were published by three different groups at about the same time. As discussed above, the point spread function of a light microscope describes how light from a point source in the sample spreads into an Airy disk in the image plane, thus making it impossible to separate two light spots very close to each other. However, for any single light spot (from a single fluorophore) that is well separated from any other spot, the absolute position can be determined with much higher accuracy than the Raleigh criterion suggests by simply fitting a Gaussian to the Airy disk to locate the center and thus the location of the fluorophore. PALM, FPALM and STORM all make use of this strategy in combination with special dyes that first need to be photoactivated by a pulse of light before becoming fluorescent. Photoactivation is stochastic, and with a sufficiently weak activation pulse only a small subset of all of the dye molecules in the field of view are activated. Thus, most fluorescing

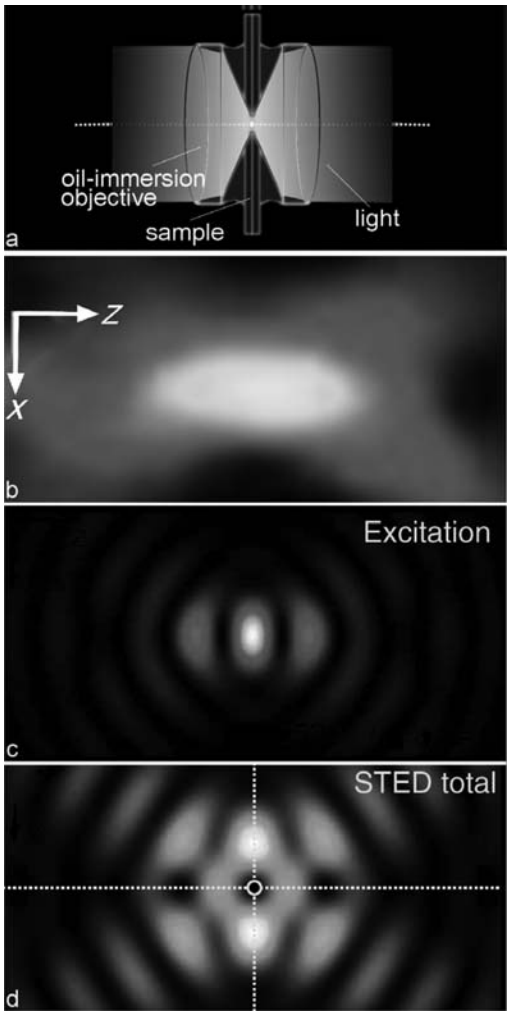

Fig. 8.6 (**a–d**) Focal intensity distributions and formation of the STED point spread function. (**a**) 4-pi microscopy. Two oil immersion objective lenses are mounted opposite to each other with the sample positioned in-between them. This results in twice the numerical aperture of a single lens, and thus improved resolution. Moreover, the focal spot can be further narrowed through constructive interference between the beams coming from opposite directions, similar to interferometry. (**b–d**) Close-ups of the light intensity distribution in the focal region. (**b**) A regular cigar-shaped focal spot from a single lens (shown for comparison). (**c**) Constructive interference pattern of excitation light in the 4-pi set-up. This light is used to excite the fluorescence in the sample. Note the favorable intensity distribution as compared to the regular PSF shown in (**b**). The situation is further improved through STED. (**d**) STED intensity distribution. This light is of a longer wavelength than the excitation light (shown in **c**) and serves to extinguish fluorescence. The STED light cuts into the excitation spot almost isotropically from all directions, sparing only a small central sphere. This sphere, with a diameter of only about 40 nm (denoted by a ring in **d**), is the only region from which fluorescence emanates, thus leading to the dramatic increase resolution of this microscopy over traditional confocal fluorescence microscopes (adapted with the permission of Macmillan Publishers Ltd. from Schmidt et al. 2008)

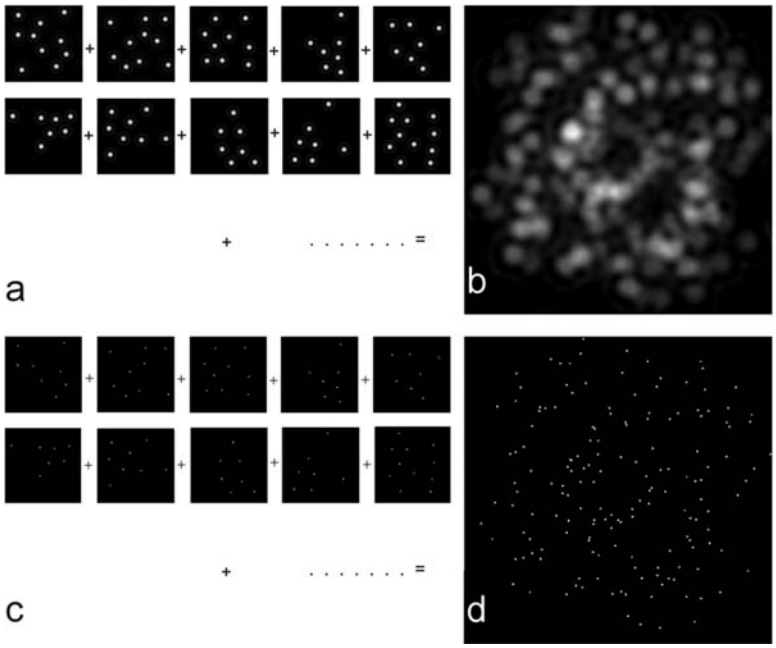

Fig. 8.7 (**a–d**) Principle of STORM/PALM/FPALM. (**a**) An activation laser pulse stochastically excites a small subset of photoactivatable fluorescent dyes to their fluorescent states. The dyes are imaged for one or a few frames until they become bleached (PALM, FPALM) or are returned to the dark state (STORM). This process is repeated, with a different subset of the dyes observed each time. Conditions are chosen so that the dye molecules are well separated from each other in the individual frames. Airy disks in individual frames are reduced to dots (**c**). The aggregate image of all frames shows that the locations of the dyes are well resolved (**d**). (**b**) A regular image of the same dye molecules included for comparison

molecules are far enough from each other to determine their locations with high accuracy.

In STORM, after acquiring a frame, all fluorescing molecules are returned to their dark states and another subset of the dyes is activated in order to acquire another frame from the same region. This process is then repeated many times (e.g., 10,000 times). Each individual frame is reduced computationally to a map of locations of individual dye molecules. Adding the maps yields the super-resolution image. The inventors of STORM report the use of a photoswitchable cyanine dye. Cy5, a common cyan dye, can be switched between a fluorescent and a stable dark state ("triplet state") by red laser light, which also excites the fluorescence. Exposure to green laser light converts Cy5 back to the fluorescent state, but only when Cy3 is close-by. Hence, the Cy3–Cy5 pair comprises an optical switch. In PALM and FPALM, photoactivatable fluorescent protein molecules are turned on and localized (to 2–25 nm). After a few consecutive frames, the dyes become bleached. The method can be used to achieve high resolution not just in the lateral dimension but also the axial direction. This is accomplished by making the objective slightly astigmatic.

An astigmatic objective focuses light in one lateral direction more strongly than in another. Any point source imaged with such lens will produce a round Airy disk only when it is in focus between the strongest and the weakest focal directions. If it is in focus in the stronger focal direction, it will be spread out in the weaker focal direction, thus producing an ellipsoid, and vice versa. Using this information, the distorted shape of the Airy disk enables the true location of each fluorophore within the image frame to be gauged not just laterally (with a precision of 20 nm) but also axially (to an accuracy of 60 nm), thus achieving resolutions well below the diffraction limit (Fig. 8.8).

All of the super-resolution light microscopy methods described above are inherently limited in terms of speed by the low rate of photon emission from a small spot as compared to the larger spots associated with regular microscopy. However, live cell imaging has still been achieved in STED at 28 frames s^{-1} for the example of the movement of synaptic vesicles in cultured neurons. This has been accomplished by reducing the spot size to a level where just enough photons from the features of interest are emitted within the given short acquisition time to allow them

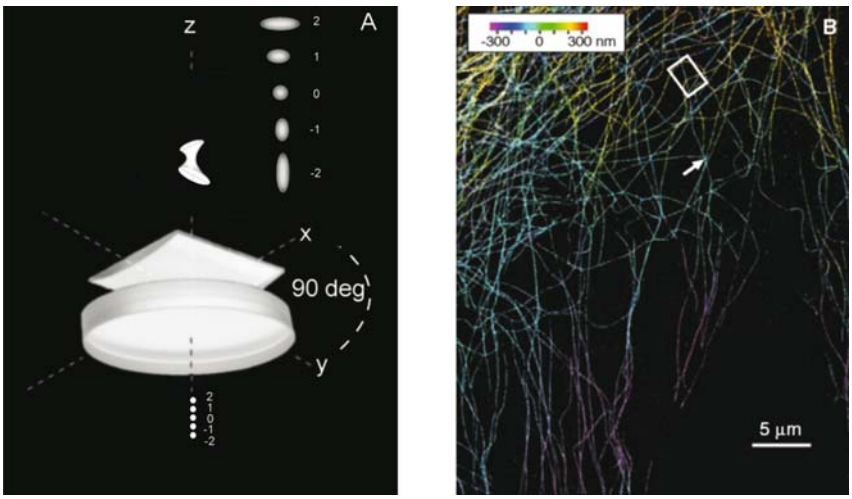

Fig. 8.8 (**a–b**) Three-dimensional (3D) STORM. (**a**) Principle. A weak cylindrical lens is added to the objective to make it astigmatic. In an astigmatic objective, the focal length in one direction (here the *x*-direction) is shorter than in another direction (*y*-direction). A fluorophore is thus imaged into an elliptical Airy disk with its main axis along the *x*-direction when it is in focus in the *x*-direction (close to the objective, denoted by 2), a circular disk when at an intermediate focal length (0), and an elliptical disk with its main axis in the *y*-direction when it is even further away from the objective (Vainrub et al. 2006) and in focus in the *y*-direction. The shapes of the Airy disks above the objective and the corresponding fluorophores below the objective are denoted by corresponding numbers. Therefore, a single image frame in 3D STORM contains not only information about the locations of all the fluorescent dyes in the image plane (x, y), but also information on the distance of each fluorophore from the objective (z-direction), as derived from the shape of its Airy disk. (**b**) Image of microtubules in a cell. The z-position information is color-coded according to the *color scale bar* (from Huang et al. 2008 and used with permission)

to be discerned from the background. PALM and FPALM have also been used in live cell imaging. The time resolution of PALM has been relatively slow for live cell imaging, and a value of 500 s/image (with an image being the aggregate information from 10,000 individual frames taken at 20 frames s^{-1}) has been reported. However, in their live cell application of PALM, Manley et al. did not use only the aggregate information. Rather, reoccurring fluorescence from individual dyes over a number of consecutive frames (before they became bleached) was mapped and the trajectories of the tagged proteins were plotted as in conventional "single-particle tracking" (spt). However, rather than tracking single ensembles of molecules, the photoactivatable fluorophores allowed multiple ensembles of molecules to be activated, imaged and bleached. Thus, several orders of magnitude more trajectories per cell were obtained as compared to conventional single-particle tracking. Hess et al. (FPALM) also made use of the reoccurrence of fluorescence from single molecules over two to four frames to study molecular dynamics. The PALM/FPALM/STORM principle has now been licensed by Zeiss and will be offered on their laser scanning confocal microscope platform LSM 710.

In summary, recent improvements in light microscopy have extended the resolution well into the realm of the ultrastructure of the cell. Lateral resolution on the order of 20 nm and axial resolution on the order of 60 nm have been convincingly demonstrated, even in living cells. At the same time, molecular motion has been observed at up to 20 frames s^{-1}. Future improvements in all super-resolution microscopy methods are entirely possible, with respect to both spatial and time resolution. Such improvements may be brought about or at least depend on brighter fluorophores.

Image processing: Image processing in advanced light microscopy is pursued in order to enhance 3D light microscopy datasets by deconvolution (discussed above), to provide a comprehensive display, and to perform a statistical data analysis, including the colocalization of cellular components in three dimensions and in time series of 3D images (termed 4D). Unlike two-dimensional images, we cannot directly display three-dimensional images on a computer screen. Therefore digital image processing is an essential component of any 3D microscope system. Moreover, quantitative data assessment is often indispensable when answering a research question.

Principally, all of the abovementioned traditional optical sectioning microscopy and super-resolution techniques produce datasets that require image processing. The following section briefly describes what image processing involves, starting with the raw data and achieving quantitative, statistically meaningful numbers. Examples are taken from one of the common image processing software packages (*Imaris* from bitplane, Zurich, Switzerland). In image processing, the first task usually consists of visualizing the data. Imaris as well as other packages offer a palette of fast operations to project the data onto a 2D screen, a process often referred to as "3D reconstruction" or "rendering" (Fig. 8.9). The projection methods include *maximum intensity projection* (MIP), which prioritizes the bright structures, and *blending* or *ray-tracing*, which prioritizes the structures close to the point of view. Software enables users to adapt the transparency, colors, and lighting to the needs of the study

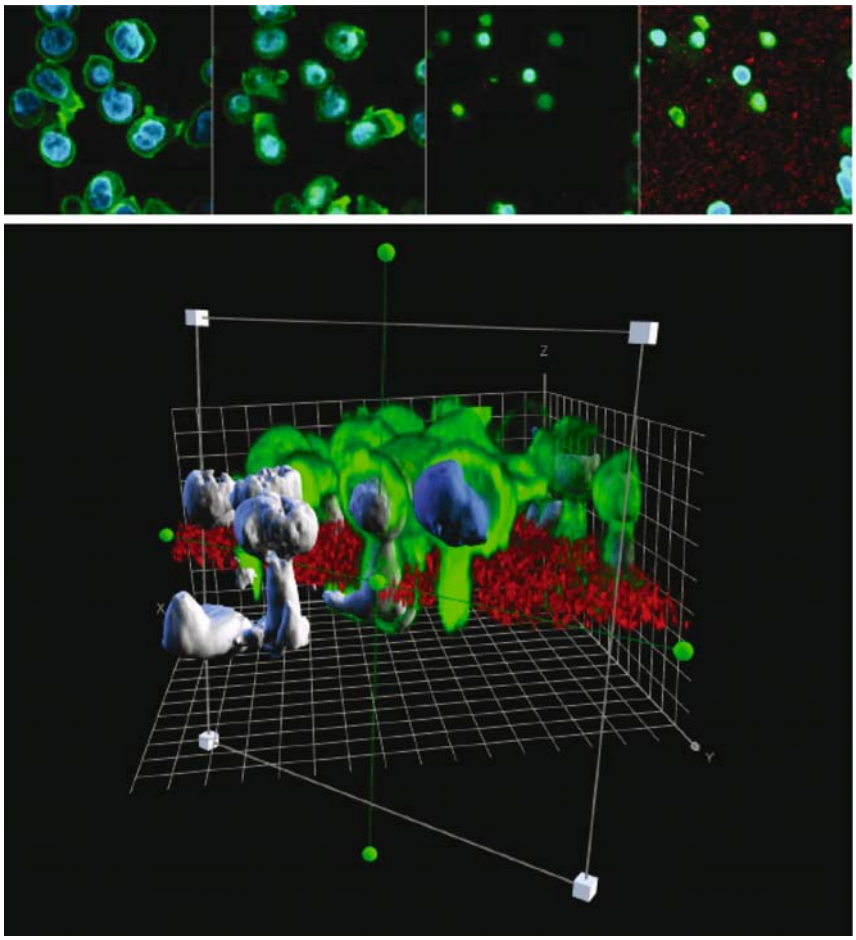

Fig. 8.9 (*Top row*) Confocal optical slices taken at four different z-planes 4.7 µm apart from each other. Actin is shown in *green*, DAPI stain (a stain of the nucleus) is shown in *blue* and an artificial membrane is shown in *red* (*bottom row*). A 3D reconstruction of 64 slices, of which four are shown above, is depicted. Only in 3D does it become apparent that the cells have migrated across the membrane. A clipping plane is positioned vertically to the plane of the membrane to expose a cross-section through the cells (image display by Imaris, data courtesy of Dr. Tomoko Shibutani, DAIICHI Pharmaceutical, Tokyo)

and the dataset. If the purpose was visualization, we may end up with a set of rendered pictures and animations showing important aspects of the 3D image. Quite often, however, visualization is used to assess the image before it is subjected to further quantitative analysis.

For many studies involving quantitative analysis, the first step is to identify objects in the image. This operation is usually referred to as "segmentation," and is one of the major steps in the analysis. The user can choose the object "detector"

that best matches the image. For instance, tiny structures such as vesicles or nuclear FISH signals would typically be detected in Imaris by the "Spots" detector component, whereas dendrite trees of neurons are detected using the Imaris "Filament" detector. The segmentation step is also where fluorescent microscopy has a large advantage over other methods such as transmission or reflection microscopy.

The ability to selectively label structures of interest combined with its suitability for 3D imaging has enormously facilitated the segmentation step. Rather than analyzing the complex patterns and edges of transmission micrographs, software can simply localize high-intensity elements in the image; these are inherently the areas of interest. Segmentation is one of the reasons why interactive software packages such as Imaris are generally favored over noninteractive software—they offer manual editing of automatically obtained results. Once segmentation has occurred, quantitative analysis of the objects can be pursued, volumes can be calculated, distances can be measured and the branching of processes can be evaluated, to name just a few examples for quantitative data analysis (Fig. 8.10).

Electron Tomography

Only recently, ultrastructure imaging was the domain of transmission electron microscopy (TEM) alone. Electron microscopy utilizes a beam of electrons that are accelerated by a high voltage and directed into vacuum column with electromagnetic lenses, rather than visible light and glass lenses. TEM thus exploits the very

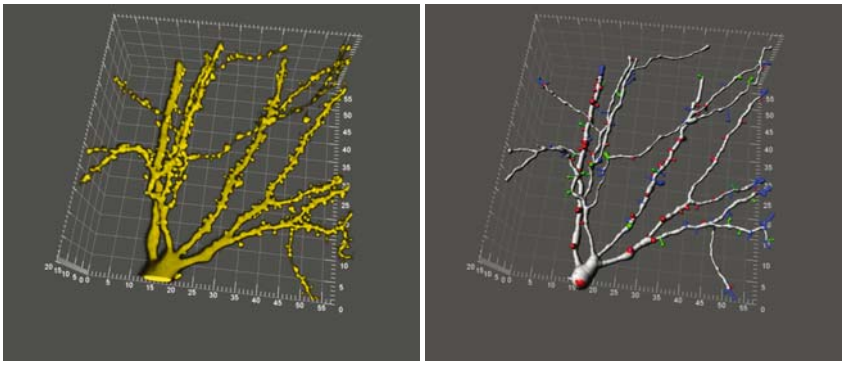

Fig. 8.10 (*Left*) A blending reconstruction of a lucifer yellow-injected single nerve cell displaying dendrites and spines. While visually informative, the software is unable to obtain quantitative information from data in this form. The figure on the (*right*) was created from the same data after automatic segmentation. The dendrites and spines were automatically segmented using FilamentTracer from Imaris, a software module designed for the analysis of longitudinal, branched structures. The data is now available as an object graph and the software is able to count branch points and to measure the lengths and diameters of each of the dendrite segments; hence the information is much more readily available for quantification (dimensions are in microns; courtesy of Anne McKinney, McGill University, Montreal)

short wavelength of the electron beam to boost the resolution of the optical system way beyond that offered by visible light. While TEM is now receiving competition from super-resolution light microscopy, it will continue to play an important role in revealing the spatial relationships of the macromolecules in cells and tissues. This is because, in light microscopy, macromolecular identity is only revealed after labeling. The large number of different proteins and other macromolecules at work at any time in a cell makes it inconceivable to extend this approach to deduce even a substantial subset of all of its macromolecular relationships by methods that depend on labeling. Moreover, even the cellular architecture of compartments separated by membranes, the cytoskeleton and the nucleus with its substructure all need labeling to be well resolved, even when using the most advanced light microscope. TEM on the other hand reveals all of the compartments in the cell directly, and much of the cytoskeleton is identified without labeling as well. Moreover, TEM is now making a strong resurgence as electron tomography (ET), a novel data collection strategy, enables explorations of cellular ultrastructure in three dimensions at very high resolution (Kurner et al. 2005; Richter et al. 2008; Marsh et al. 2001; McIntosh et al. 2005; Lucic et al. 2005).

Electron tomography has been developed over more than 20 years. However, the technology has only just now matured to the point where it can be routinely applied to specimens in a fully automated fashion. This not only makes the recording of tomographic datasets much less cumbersome, but it also makes it possible to minimize the exposure of the specimen to the electron beam, a major concern in the high-resolution TEM of inherently beam-sensitive biological specimens. In traditional TEM, a single projection image (micrograph) of the region of interest in a thin section is acquired with the specimen positioned perpendicular to the electron beam. In the process of electron tomography, on the other hand, several hundred digital micrographs are acquired, each from a different viewing direction, as the specimen is rotated around the region of interest from about 70° tilt angle from its normal to the beam, through zero, to −70°. The resulting set of micrographs is computationally back-projected into a single 3D object, according to the same concepts as used in medical computer tomography or other tomographic methods (Fig. 8.11).

The tomogram allows for a much more comprehensive structure-based understanding of the role of the proteins of interest in their cellular context than traditional electron micrographs. In addition to revealing ultra- and molecular structure in three dimensions (which is far more meaningful), it greatly (or significantly) increases the information obtained in the viewing direction over the traditional single projection. In a single micrograph, all of the structures in the viewing direction overlap and the resolution is basically reduced to the thickness of the complete specimen, e.g., the thickness of a plastic section of some cells or tissue, whereas the resolution is almost isotropic in all directions after tomography. The current resolution of cell organelles, subcellular assemblies and, in some cases, whole cells permitted by ET is in the range 5–20 nm: suitable for identifying supramolecular multiprotein structures in their cellular context (Fig. 8.12). However, in order to identify it in a tomogram, the shape of such supramolecular structure must be known beforehand; from X-ray crystallography, NMR spectroscopy, EM crystallography or single-particle analysis

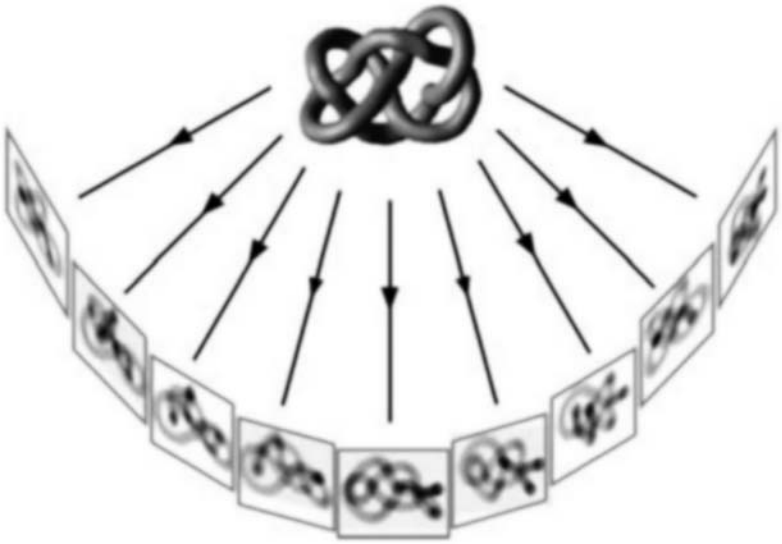

Fig. 8.11 In electron tomography (ET), many projected images of a sample are acquired. In order to achieve this, the sample is tilted with respect to the beam in-between images. The 3D structure of the object is then reconstructed from the individual micrographs through computational "back projection" (from Lucic et al. 2005 and used with permission)

(Medalia et al. 2002). The known shape of the complex is then used as a "mask" in an algorithm that is designed to locate copies of it within a tomogram via cross-correlation. ET also reveals the context of protein complexes with other cellular components, such as DNA and membranes.

The high resolution offered by ET naturally depends on adequate sample preservation for the improved resolution to be meaningful. During processing, samples are rendered compatible with the high vacuum of the microscope, and they are often cut into sections that are sufficiently thin for the electron to beam to penetrate. Tissues or cells may be fixed chemically, embedded in plastic and cut into thin sections by an ultra microtome. Some heavy metal staining is usually introduced to surround the molecules and thus improve contrast. Modern TEM performed with an "intermediate" acceleration voltage for the beam electrons of 200–300 kV allows samples up to about 200–300 nm thick to be penetrated. Similar, although thinner, sections are also used widely in traditional TEM to study the morphology, ultrastructure, and contents of cells and their subcellular organelles. However, chemical fixation may not sufficiently preserve the structures for ET. To greatly improve structure preservation, samples can be rapidly frozen employing special procedures to prevent ice crystals from forming: this is an artefact-free fixation method. Frozen specimens can then be processed by "freeze substitution." In this process, the water in the frozen specimen is gradually replaced with a plastic resin at low temperature so that all structures are retained in place throughout. After polymerizing the resin, the samples are sectioned in a similar way to chemically fixed samples. In a variant of this

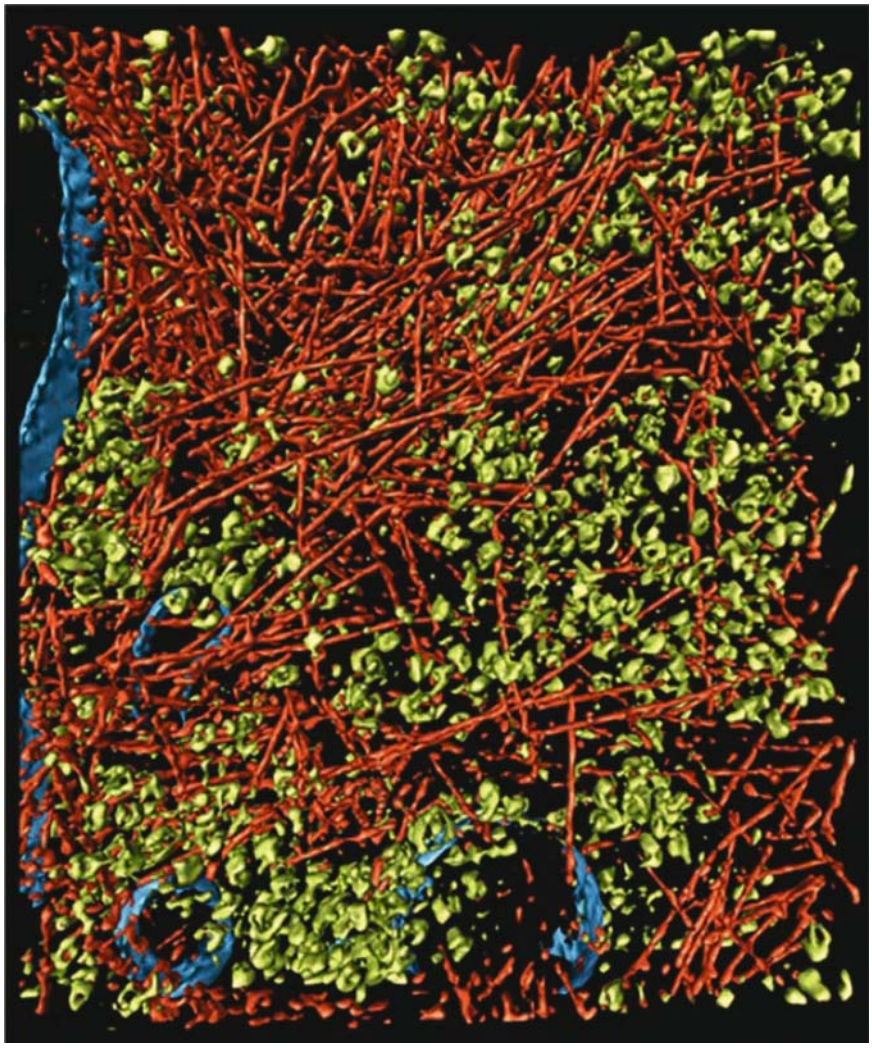

Fig. 8.12 Surface rendering of an actin network, membranes, and cytoplasmic macromolecular complexes ($815 \times 870 \times 97$ nm). The actin filaments are *reddish*, the ribosomes *green* and the membranes *blue* (from Medalia et al. 2002 and used with permission)

approach, the frozen sample can also be cut directly into thin sections for cryo-TEM without plastic embedding or staining. However, cryosections are difficult to obtain as they tend to crack because of the compression caused by commonly used diamond knifes. Better results have recently been achieved by carving sections out of a frozen sample by focused ion beam thinning (i.e., exposing the frozen sample to an ion beam in order to sputter material). Notwithstanding the great technical challenges posed by obtaining and imaging cryosections, excellent results have been obtained from bacteria samples, particularly in terms of the preservation of

membrane structure and extracellular glycoprotein architecture (Marko et al. 2007). In other cases, the specimens are within the required 200–300 nm thickness or are not much greater than this, so sectioning is not required. This may be true for extended processes of cells or for large regions of epithelial or endothelial cells. The cells can be cultured directly on a thin carbon or plastic film used as a support during the microscopy; this is then frozen and introduced into the microscope (Medalia et al. 2002).

ET has matured at a time when electron microscopes have also improved greatly, meaning that the information about the object carried by the electron beam is almost fully exploited. However, the ultimate resolution of electron microscopy and hence ET is inherently limited due to the damage that occurs when electrons interact with the cellular structure. Current resolutions may indeed be close to a "theoretical" limit, and this would mean that the secondary and tertiary structure of an individual protein or polypeptide would remain out of bounds. The identification of proteins that are not in large complexes would therefore continue to require (immunogold) labeling.

Atomic Force Microscopy

AFM does not depend on light or optics. In AFM, the topology of a sample is traced by a sharp stylus that is scanned line by line over the sample. The stylus sits at the free end of a cantilever spring and lightly touches the sample. Increases in elevation of the sample cause the stylus to move up and bend the cantilever upward while depressions allow the stylus to move down. The stylus and cantilever are usually microfabricated from silicon or silicon nitrite. The cantilever is typically a fraction of a millimeter long and a few micrometers thick. AFM lends itself well to imaging molecular and cellular specimens under physiological conditions in buffer. The AFM cannot look inside an intact cell, but it can be used to either investigate elements of the ultrastructure that have been isolated or to probe the outer surfaces of cells.

When imaging isolated molecular assemblies, AFM offers very high resolution at a high signal-to-noise ratio. Biological membranes for example can be imaged in their native state at a lateral resolution of 0.5–1 nm and a vertical resolution of 0.1–0.2 nm. Conformational changes that are related to functions can be resolved to a similar level. This is well beyond the capabilities of any other microscope (Fig. 8.13).

In addition to imaging the structure, AFM can map properties of the sample such as local stiffness, electrical conductivity or electric surface potential (Fig. 8.14). In the example given in Fig. 8.14, the map of the electric surface potential helped to reveal the local molecular arrangement of pulmonary surfactant (Leonenko et al. 2007a, b).

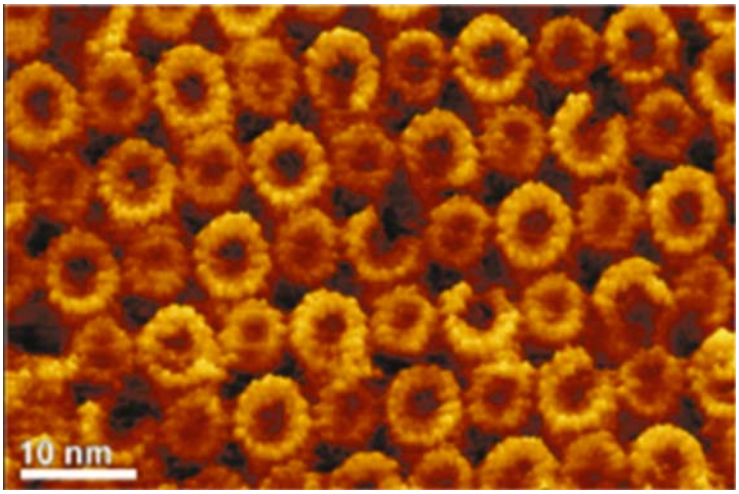

Fig. 8.13 ATP synthase is a proton-driven molecular motor with a stator (seen here) and a rotor. It has not yet even been possible to count the number of individual proteins inside the ring structure based on electron micrographs (adapted with the permission of Macmillan Publishers Ltd. from Seelert et al. 2000)

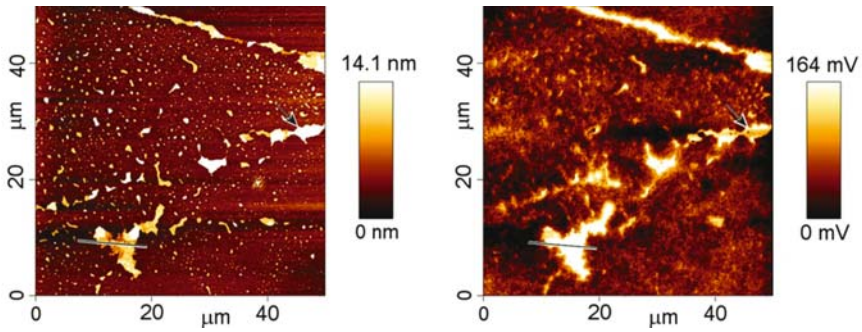

Fig. 8.14 A film of pulmonary surfactant. The topographical image (*left*) shows a pattern of lipid monolayer and scattered multilayer regions (stacks of lipid bilayers). In the potential map (*right*), large stacks of bilayer patches are at a potential of up to 200 mV above the monolayer. We associated the positive surface potential of the stacks with the presence of the surfactant-associated protein C (SP-C). The helical structure of SP-C constitutes a strong molecular dipole (taken from Leonenko et al. 2001 with permission; the image was taken with a NanoWizardII AFM from JPK Instruments, Berlin)

AFM started out as an imaging tool, and early applications demonstrated the resolution power and high signal-to-noise ratio that it offers at the macromolecular level. Although unintentionally at first, it soon became clear that the probe could be used to manipulate and probe macromolecular structures individually, thus opening up a wide range of applications for this technology. The most notable of these is termed "force spectroscopy" (Fig. 8.15). It is based on the fact that the force between

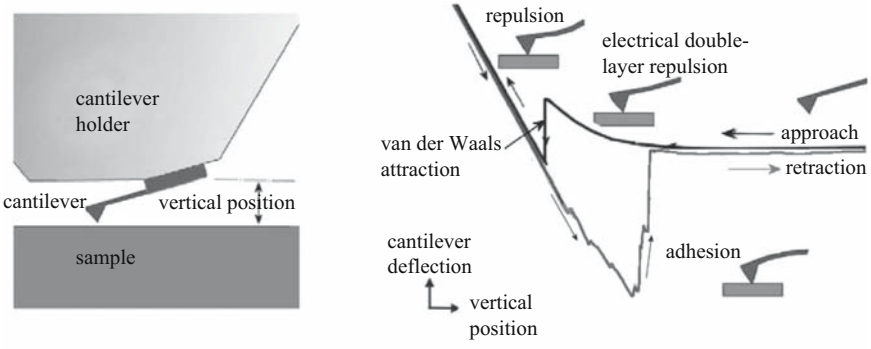

Fig. 8.15 Force vs. distance curve. For the example shown here, the tip first experiences a long-range repulsive force upon approaching the sample, even before the tip and sample are in physical contact. Close to the sample, the tip becomes strongly attracted by the van der Waals force. In this instance, the attractive force gradient becomes greater than the force associated with the cantilever spring. This causes the tip to snap into physical contact with the sample (the perpendicular part of the approach curve). Once physical contact has been made, the cantilever is deflected linearly by the approaching scanner until the scanner stops. On the way back, the tip often sticks to the sample by adhesion until the pull from the cantilever forces it out of contact. The adhesion curve is often the most interesting part. It can reveal the folding path of a protein, be used to measure immune cell activation, or show the time dependence and progression of nanoparticle uptake by lung epithelial cells (Fig. 8.16), to name but a few examples

the stylus and sample derives from not only the active loading of the stylus onto the sample, but also the interactions that occur between the sample and the tip, including van der Walls, ionic and hydrophobic interactions. These interactions are the same as those that rule molecular interactions in cells and tissues, including nonspecific interactions and highly specific receptor–ligand interactions (Israelachvili 1997). The forces they produce typically range from a few piconewtons to a few nanonewtons and are thus well within the measurement accuracy of the AFM.

For a number of examples, molecular images have been obtained with sufficient resolution to individually recognize single macromolecules and then address the molecules individually with the stylus of the AFM. Single-molecule force spectroscopy combined with single-molecule imaging has provided an unprecedented means to analyze intramolecular and intermolecular forces, including those involved in the folding pathways of proteins. Probing the self-assembly of macromolecular complexes and measuring the mechanical properties of macromolecular "springs" are other examples of where AFM has made substantial contributions to the life sciences.

The imaging of living cells with AFM is performed in conjunction with local probing of the sample (Figs. 8.16 and 8.17). The images by themselves are usually only used to obtain proper experimental control. The extreme flexibility of the cell membrane means that the images often show a combination of the cell topography and the mechanical stiffness of cytoskeletal fibers and vesicles below the cell surface. The in situ probing of the responses of cells to electrical, chemical or mechanical stimulation is also possible.

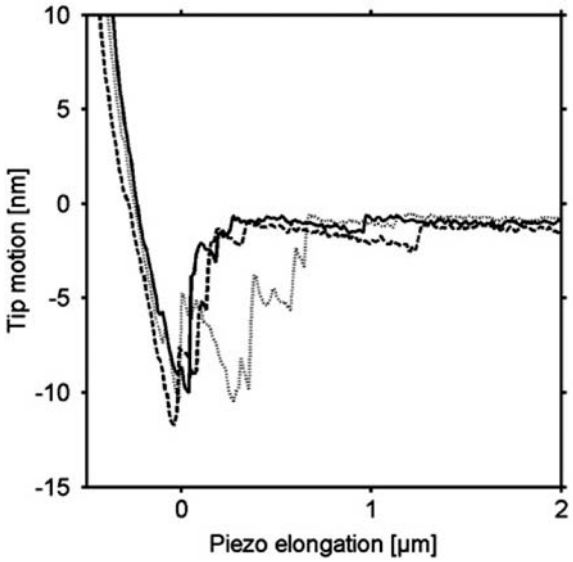

Fig. 8.16 Force vs. distance curve of a chemically modified AFM stylus on a lung epithelial cell (adapted from Leonenko et al. 2007a, b and used with permission from Elsevier). Here, the AFM tip serves as a model of a nanoparticle that enters the lung via the ambient air and is taken up by the body. The study revealed the important aspects of the particle uptake by measuring the time-dependent adhesion of the particle to the plasma membrane

Future Directions in Ultrastructure Imaging

Knowing at any given time where every atom of every molecule resides in an organism holds the key to answering any research question in the life sciences. Our current understanding is that the combination of crystallography or NMR (which reveal the atomic structures of macromolecules), electron tomography (which allows the determination of the precise subcellular positions and interactions of macromolecular machines), and fluorescence light microscopy (which describes the dynamic nature of cellular processes) should lead to a profound understanding of the cellular processes associated with the physiological functions of tissues and organs and the pathogenesis of disease. However, the sheer number of macromolecules in an organism or even in a single cell that are interacting and being modified and turned at any given time, not to mention the small molecules of the "metabolome," makes the notion of obtaining the entirety or even a substantial fraction of the mechanics of a cell, tissue or organism with current techniques quite inconceivable. Gene array technology that is designed to reveal cellular responses to even small interferences with normal cell function typically returns hundreds of changes in gene activity, some of which are anticipated but many of which are entirely unexpected and in no way understood. This is testament to the level of integration and interdependence of the molecular construction of cells. Hence, by observing hundreds or thousands

Fig. 8.17 A neuron cultured on an electronic chip. The chip is designed to pick up an action potential from the cell. The image demonstrates the proper tracing of the cell surface. In a future application, an appropriately designed stylus could be used as an additional electrode to excite or record an action potential at any location on the cell body or a neuronal cell process

of different molecular species at a time by microscopy, one ought to be able to do justice to the complexity of life, or, in more practical terms, efficiently unravel the molecular pathways associated with a function of interest. Such an approach would be conceptually similar to the systematic, unbiased approaches of genomics and proteomics. No single existing microscopy technique that is currently in existence or even any combination of all of them has the potential to achieve this. On the other hand, current analytical tools for identifying large numbers of molecular species at a time—with mass spectrometry being one important example—are not designed to determine the part of a cell in which a particular molecule is located. An ideal microscope would combine the high level of localization of today's ultrastructure imaging tools and the capabilities of mass spectrometry (for example, the ability to identify

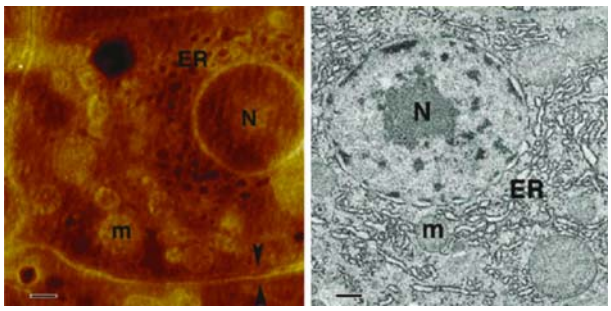

Fig. 8.18 AFM of cell sections (*left*); for comparison a TEM micrograph of the same specimen is also shown (*right*). AFM and TEM both give a highly detailed image of the cell's ultrastructure. *N*, nucleus; *ER*, endoplasmatic reticulum; *m*, mitochondria (adapted from Matsko and Mueller 2004 with permission)

molecular species based on their own characteristics rather than via labeling). Such a microscope is yet to be invented.

Among all current microscopic techniques, AFM may offer one avenue to such a microscope. It has recently been demonstrated that thin sections of fixed and embedded tissue and cell samples make the cell's interior accessible to AFM. High-resolution cell images give a clear image of the cell's ultrastructure, sometimes reaching down to the macromolecular level (Fig. 8.18). While the AFM is unlikely to allow macromolecules to be identified by shape, it could be combined with powerful local spectroscopy. The stylus could then act as both an imaging tool and a local spectroscopic probe. One can speculate that spectroscopy might lend the microscopy the ability to identify macromolecular specimens under the tip directly.

In summary, the past few years have seen dramatic improvements in life science microscopy. Super-resolution fluorescence light microscopy has permitted the ultrastructure imaging of living cells. In electron tomograms, macromolecular complexes can be identified directly by shape, without the need for labeling. Atomic force microscopes image isolated elements of the ultrastructure, including membranes and macromolecules, at submolecular resolution. This technology also makes molecular interactions directly accessible through the measurement of binding forces. Finally, there is still room for further invention—a microscope that does not require the use of labeling to identify molecules, from metabolites to macromolecules within the ultrastructure of the cell, is not yet on the horizon.

Acknowledgments The author is grateful to Dr. Mary Brindle and Dr. Michael Schoel for their critical reading. We thank Dr. Marius Messerli for his assistance in preparing the section on image processing and for providing the figures associated with that section. The "neuron on a chip" shown in Fig. 8.17 was prepared by the laboratory of Dr. Naweed Syed. We acknowledge the permission to reproduce the diagrams and images shown in Figs. 1, 4–6, 8, 11–14, 16 and 18.

References

Betzig E, Patterson GH, Sougrat R, Lindwasser OW, Olenych S, Bonifacino JS, Davidson MW, Lippincott-Schwartz J, Hess HF (2006) Imaging intracellular fluorescent proteins at nanometer resolution. Science 313:1642–1645

Conchello JA, Lichtman JW (2005) Optical sectioning microscopy. Nat Methods 2:920–931

Hammond C, Heath J (2006) Symmetrical ray diagrams of the optical pathways in light microscopes. Microsc Anal 115:5

Hess ST, Girirajan TPK, Mason MD (2006) Ultra-high resolution imaging by fluorescence photoactivation localization microscopy. Biophys J 91:4258

Hess ST, Gould TJ, Gudheti MV, Maas SA, Mills KD, Zimmerberg J (2007) Dynamic clustered distribution of hemagglutinin resolved at 40 nm in living cell membranes discriminates between raft theories. Proc Natl Acad Sci USA 104:17370–17375

Huang B, Wang W, Bates M, Zhuang X (2008) Three-dimensional super-resolution imaging by stochastic optical reconstruction microscopy. Science 319:810–813

Israelachvili JN (1997) Intermolecular and surface forces. Academic Press, London

Kurner J, Frangakis AS, Baumeister W (2005) Cryo-electron tomography reveals the cytoskeletal structure of spiroplasma melliferum. Science 307:436–438

Leonenko Z, Gill S, Baoukina S, Monticelli L, Doehner J, Gunasekara L, Felderer F, Rodenstein M, Eng LM, Amrein M (2007a) An elevated level of cholesterol impairs self-assembly of pulmonary surfactant into a functional film. Biophys J 93:674–683

Leonenko Z, Finot E, Amrein M (2007b) Adhesive interaction measured between AFM probe and lung epithelial type II cells. Ultramicroscopy 107:948–953

Leonenko Z, Finot E, Leonenko Y, Amrein M (2008) An experimental and theoretical study of the electrostatic interactions between pulmonary surfactant and airborne, charged particles. Submitted for publication

Lucic V, Forster F, Baumeister W (2005) Structural studies by electron tomography: From cells to molecules. Annu Rev Biochem 74:833–865

Manley S, Gillette JM, Patterson GH, Shroff H, Hess HF, Betzig E, Lippincott-Schwartz J (2008) High-density mapping of single-molecule trajectories with photoactivated localization microscopy. Nat Methods 5:155–157

Marko M, Hsieh C, Schalek R, Frank J, Mannella C (2007) Focused-ion-beam thinning of frozen-hydrated biological specimens for cryo-electron microscopy. Nat Methods 4:215–217

Marsh BJ, Mastronarde DN, Buttle KF, Howell KE, McIntosh JR (2001) Organellar relationships in the golgi region of the pancreatic beta cell line, HIT-T15, visualized by high resolution electron tomography. Proc Natl Acad Sci USA 98:2399–2406

Matsko N, Mueller M (2004) AFM of biological material embedded in epoxy resin. J Struct Biol 146(3):334–343

McIntosh R, Nicastro D, Mastronarde D (2005) New views of cells in 3D: an introduction to electron tomography. Trends Cell Biol 15:43–51

Medalia O, Weber I, Frangakis AS, Nicastro D, Gerisch G, Baumeister W (2002) Macromolecular architecture in eukaryotic cells visualized by cryoelectron tomography. Science 298:1209

Perfect Storm A (2008) Colour-controllable LEDs, three-dimensional fluorescence nanoscopy, medical nanotags, and more. Science 319:810–813

Richter T, Floetenmeyer M, Ferguson C, Galea J, Goh J, Lindsay MR, Morgan GP, Marsh BJ, Parton RG (2008) High-resolution 3D quantitative analysis of caveolar ultrastructure and caveola-cytoskeleton interactions. Traffic 9(6):893–909

Rust MJ, Bates M, Zhuang X (2006) Sub-diffraction-limit imaging by stochastic optical reconstruction microscopy (STORM). Nat Methods 3:793–795

Schmidt R, Wurm CA, Jakobs S, Engelhardt J, Egner A, Hell SW (2008) Spherical nanosized focal spot unravels the interior of cells. Nat Methods 5:539–544

Seelert H, Poetsch A, Dencher NA, Engel A, Stahlberg H, Muller DJ (2000) Structural biology. Proton-powered turbine of a plant motor. Nature 405:418–419

Shroff H, Galbraith CG, Galbraith JA, Betzig E (2008) Live-cell photoactivated localization microscopy of nanoscale adhesion dynamics. Nat Methods 5:417–423

Vainrub A, Pustovyy O, Vodyanoy V (2006) Resolution of 90 nm (lambda/5) in an optical transmission microscope with an annular condenser. Opt Lett 31:2855–2857

Willig KI, Rizzoli SO, Westphal V, Jahn R, Hell SW (2006) STED microscopy reveals that synaptotagmin remains clustered after synaptic vesicle exocytosis. Nature 440:935–939

http://www.springer.com/978-3-540-68992-8

Advanced Imaging in Biology and Medicine
Technology, Software Environments, Applications
Sensen, C.W.; Hallgrimsson, B. (Eds.)
2009, XII, 445 p. 164 illus., 103 illus. in color.,
Hardcover
ISBN: 978-3-540-68992-8